Journal of The Electrochemical Society, **151** (7) F162-F165 (2004)
0013-4651/2004/151(7)/F162/4/$7.00 © The Electrochemical Society, Inc.

High-Density RF MIM Capacitors Using High-*k* La_2O_3 Dielectrics

M. Y. Yang, D. S. Yu, and Albert Chin[z]

Department of Electronics Engineering, National Chiao Tung University, Hsinchu 30010, Taiwan

The integrity of the metal-insulator-metal (MIM) capacitor with high-*k* La_2O_3 dielectrics formed using a 400°C back-end process was investigated. A very high capacitance per unit area of 9.2 fF/μm^2 was achieved for La_2O_3 MIM capacitors at 1 MHz, significantly reducing the chip size of radio frequency (rf) circuits. A mathematical derivation, involving measured *S* parameters, yielded the small voltage-dependent capacitance ($\Delta C/C$) $\leqslant$ 100 ppm at 1 GHz, indicating that the precision capacitor circuit can be applied in the rf regime. Furthermore, such a high capacitance density can be maintained as the frequency is increased from 10 KHz to 20 GHz with a large *Q* factor $\geqslant$90.
© 2004 The Electrochemical Society. [DOI: 10.1149/1.1752935] All rights reserved.

Manuscript submitted July 7, 2003; revised manuscript received January 9, 2004. Available electronically May 20, 2004.

As the very large scale integration (VLSI) technology continues to be scaled down, both the cutoff frequency f_T and the device size of radio frequency (rf) metal-oxide-semiconductor field-effect transistors (MOSFETs) are improved, allowing them to be used in wireless communication.[1-3] However, the chip size and cost of rf circuits cannot be greatly scaled down because nonscaled passive rf devices usually occupy a larger area than active MOSFETs. Among various passive devices, metal-insulator-metal (MIM) capacitors[4-11] are widely used in rf circuits for impedance matching and direct current (dc) filtering; they occupy a large fraction of the circuit area. Hence, a higher capacitance per unit area is required to reduce size and cost. Since the capacitance density of a MIM capacitor equals $\epsilon_0 k/t_d$, the use of a metal oxide with a high dielectric constant (k)[12-19] and the reduction of the thickness of the dielectric (t_d) are methods for increasing the capacitance density. However, the use of a high-*k* dielectric is preferred because reducing t_d exponentially increases the capacitor leakage current density and the loss-tangent due to electron tunneling. As well as having a higher *k*, such dielectrics must be of good quality with low defect density related leakage current when formed at 400°C and used for the VLSI back-end process integration.[16] The authors have already demonstrated the good rf performance of high-*k* Al_2O_3 ($k \sim 9-10$) and $AlTaO_x$ dielectrics.[15,16,19] This work further examines high-*k* La_2O_3 dielectrics from intermediate to rf frequencies. The La_2O_3 dielectric provides the special advantage of having a higher *k* than other high-*k* dielectrics.[12] The voltage-dependent capacitance change ($\Delta C/C$) of La_2O_3 capacitors decreases rapidly to a small value $\leqslant$100 ppm as the frequency is increased into the gigahertz regime. Hence, these high-*k* dielectric capacitors can be used in precision circuits at rf frequencies[20] with a large *Q* factor $\geqslant$90.

Experimental

MIM capacitors were fabricated using 4 in. p-type Si wafers. A 500 nm layer of isolation-oxide was first deposited on Si wafers to integrate the high-*k* capacitors into the VLSI back-end process. The bottom electrode of the MIM capacitor was formed on the isolation-oxide using Pt/Ti bilayer metals. The bottom electrode was also patterned to generate the coplanar transmission line for rf measurements. Then, high-*k* La_2O_3 was formed by depositing La metals on the Pt electrode, oxidizing at 400°C[15] for 45 min, and then annealing for 15 min. The above process meets the low thermal budget requirement of current VLSI backend integration. La_2O_3 dielectrics with thicknesses of 22 and 29 nm were formed. Then, Al metal was deposited on the high-*k* dielectrics, and patterning to form the top electrode of the MIM capacitor and the coplanar transmission line for rf measurements. The typical area of the MIM capacitor was 50 × 50 μm. The properties of the La_2O_3 capacitors were measured using an HP4284A precision inductor-capacitor-resistor (LCR) meter at frequencies from 10 KHz to 1 MHz, and the *S* parameters were measured using an HP8510C network analyzer at frequencies from 200 MHz to 20 GHz. Standard de-embedding was performed, and a through transmission line[21-23] was also de-embedded to reduce the parasitic series inductance to cause resonance.

Results and Discussion

DC leakage current characteristics.—Figure 1 plots the leakage current density *vs.* voltage (*J-V*) characteristics of La_2O_3 MIM capacitors. The leakage current falls rapidly as the thickness of the dielectric increases, because of electron tunneling. The asymmetry of the *J-V* characteristic at different polarity bias voltage follows from the different work functions of the top Al and bottom Pt electrodes. The leakage current density of 22 nm La_2O_3 capacitors at −1 V is $<10^{-5}$ A/cm^2. The relatively high leakage current is measured in La_2O_3 because of simple fabrication process. The results obtained for the authors' previously made $AlTaO_x$ MIM capacitor[15] were also higher than those for the Ta_2O_5 grown by advanced atomic-layer chemical-vapor-deposition (ALCVD). However, the capacitance density plotted in Fig. 2 is very high, 9.2 fF/μm^2, so the leakage current density is still sufficiently low to be used in rf circuits. The leakage current density can be further reduced using advanced ALCVD. For a typical, large capacitor of 10 pF used in rf circuits, leakage currents of under 10^{-10} A were obtained, comparable or even slightly lower than the leakage currents in deep submicrometer MOSFETs.[3,4] Notably, as VLSI technology continues to be scaled down to the 90 nm node, the operating voltage of the circuit falls only to 1.2 V.[24] This lower operating voltage and higher operating speed of MOSFETs and circuits are important advantages that reduce the energy-delay product. The lower operating voltage also helps to increase the capacitance density of MIM capacitors without the need for very thick dielectrics.

C-V characteristics at intermediate frequencies from 10 KHz to 1 MHz.—For precision analog circuit applications, MIM capacitors must be effective over a wide range of frequencies. Figure 2 plots the capacitance density *vs.* voltage (*C-V*) characteristics of La_2O_3 MIM capacitors. At 1 MHz, high capacitance densities of 9.2 and 6.9 μF/cm^2 are measured for La_2O_3 capacitors with physical thicknesses of 22 and 29 nm, respectively. The corresponding *k* values are 23 for La_2O_3 dielectrics. *C-V* data at over 1 MHz are derived from measured *S* parameters and equivalent circuit models, considered in a later section.

The capacitance variation, voltage-dependent capacitance ($\Delta C/C$), is important in precision circuit applications, so $\Delta C/C$ is determined from the plotted *C-V* measurements. Figure 3a and b plot $\Delta C/C$ for La_2O_3 MIM capacitors, with physical thicknesses of 22 and 29 nm, respectively. The $\Delta C/C$ data below 1 MHz are taken from the *C-V* plot in Fig. 2, while those above 1 MHz are taken

[z] E-mail: achin@cc.nctu.edu.tw

Downloaded on 2014-04-27 to IP 140.113.38.11 address. Redistribution subject to ECS terms of use (see ecsdl.org/site/terms_use) unless CC License in place (see abstract).

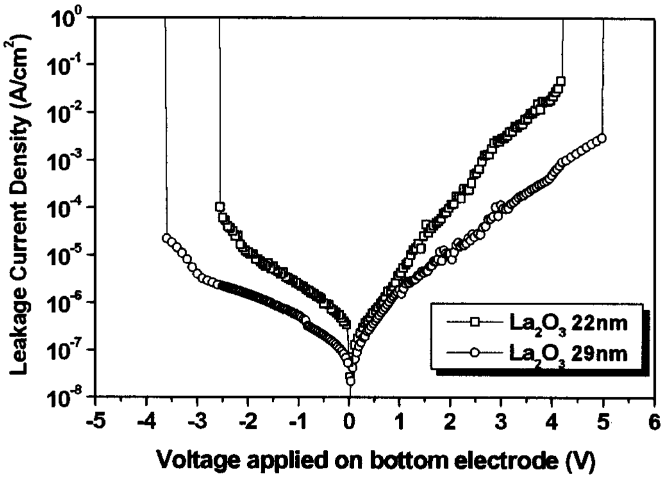

Figure 1. *J-V* characteristics of MIM capacitors with 22 and 29 nm La_2O_3 dielectrics. Asymmetry of *J-V* and breakdown voltage are related to the large difference between the work functions of Pt and Al.

from the measured *S* parameters shown below and from the authors' previously derived equations.[14] The asymmetry of the $\Delta C/C$ is caused by the difference between the top Al and bottom Pt electrodes, as in the case of the asymmetry in the *J-V* characteristics, plotted in Fig. 1. Notably, although $\Delta C/C$ is high at 10 KHz, it falls dramatically to a value of ~100 ppm as the frequency is increased to above 1 GHz. Notably, the $\Delta C/C$ results are better than were obtained for $AlTaO_x$,[15] and important for analog circuit matching.

Figure 4 plots $\Delta C/C$ and quadratic voltage coefficient, α, against frequency to elucidate further the frequency dependence of $\Delta C/C$ and related α. The relationship between α and $\Delta C/C$ is expressed as follows

$$\Delta C/C = \alpha V^2 + \beta V \qquad [1]$$

The term β is the linear voltage coefficient, and is less important than α according to the circuit cancellation method.[20] Again, $\Delta C/C$ and α fall monotonically as the frequency is increased. Small $\Delta C/C \leqslant 100$ ppm and $\alpha \leqslant 130$ ppm/V^2 are obtained as the frequency is increased into the gigahertz regime, implying that the high-*k* MIM capacitors can be used in precision circuits at operating frequencies into the gigahertz regime. High-*k* HfO_2 MIM capacitors

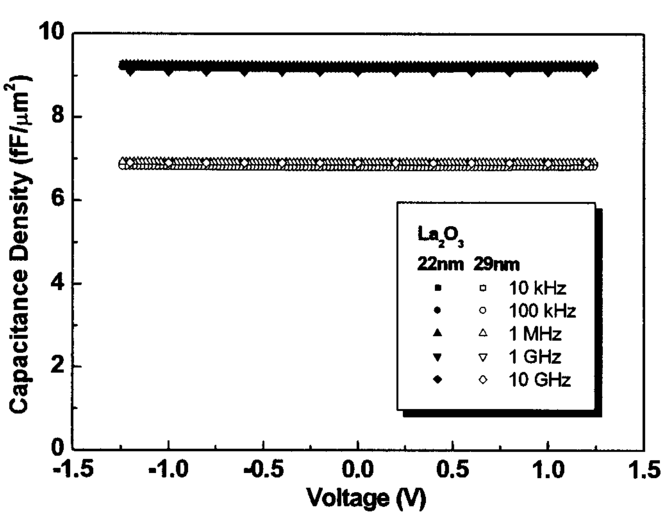

Figure 2. C-V characteristics of MIM capacitors with 22 and 29 nm La_2O_3 dielectrics at various frequencies.

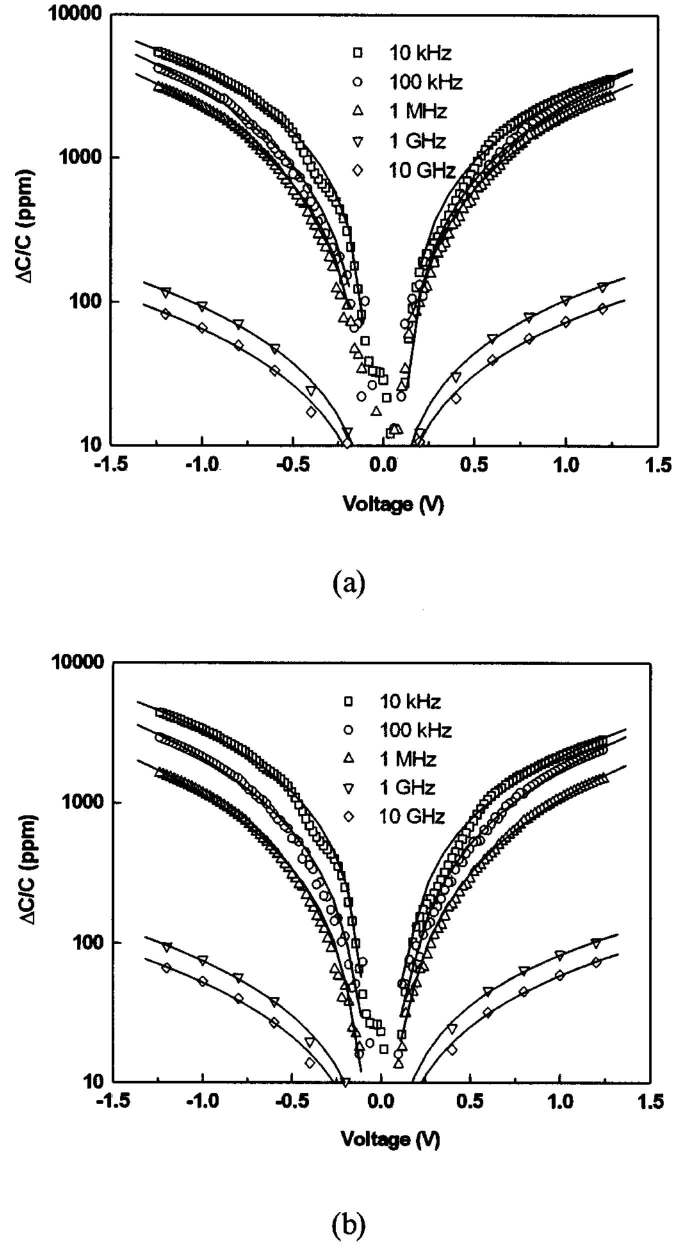

Figure 3. $\Delta C/C$ of (a) 22 and (b) 29 nm La_2O_3 MIM capacitors as functions of applied voltage at various frequencies.

also exhibit declining $\Delta C/C$ and α as the frequency rises to 1 MHz;[20] a possible mechanism for this frequency dependence is the change in the relaxation time in the high-*k* dielectric, since the carriers inside the high-*k* dielectric cannot follow the switching signal at very high signal frequencies.[20] This model also explains the continuous decrease in $\Delta C/C$ and α as the frequency increases into the gigahertz regime. Notably, the current rf circuits presently used in wireless communication are in the gigahertz regime (0.9–1.9 GHz for handset, 2.4 GHz for Bluetooth, 5.2–5.7 GHz for wireless LAN, and 3.1–10.6 GHz for ultrawide band). Hence, $\Delta C/C$ in the gigahertz regime is extremely important in both current and future rf communication.

Weak dependence of capacitance on temperature is also an important factor in circuit application. Figure 5 plots the $\Delta C/C$ of La_2O_3 MIM capacitors as functions of temperature. The temperature-dependent $\Delta C/C$ declines as frequency increases, in a

Downloaded on 2014-04-27 to IP 140.113.38.11 address. Redistribution subject to ECS terms of use (see ecsdl.org/site/terms_use) unless CC License in place (see abstract).

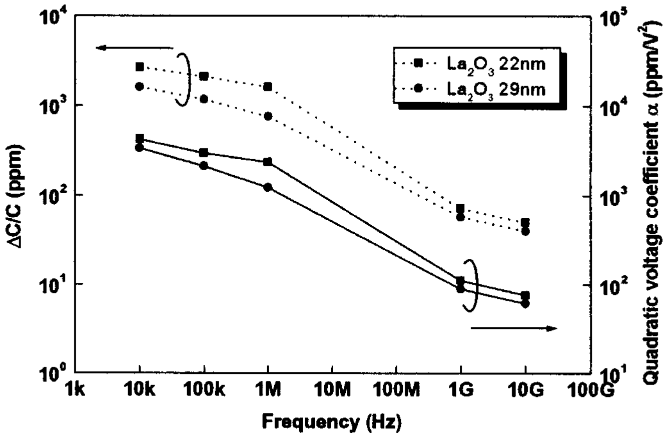

Figure 4. $\Delta C/C$ and α of La_2O_3 and $AlTaO_x$ MIM capacitors as functions of frequency.

manner consistent with Fig. 3. The $\Delta C/C$ increases with temperature, exhibiting the same trend as other dielectric capacitors published in the literature.[7]

S-parameters and rf analysis from 200 MHz to 20 GHz.—The maximum frequency at which conventional *C-V* measurements can be made using a precision LCR meter is only 1 MHz; the capacitance *C* and $\Delta C/C$ at rf frequency must be extracted from measured *S* parameters. Figure 6a and b plot the measured *S* parameters of 22 and 29 nm La_2O_3 MIM capacitors, respectively. Figure 7 shows the equivalent circuit model for MIM capacitors. Figure 2 and 3 also present extracted *C* and derived $\Delta C/C$ using our previously published equations and measured *S* parameters at 1 and 10 GHz. The $\Delta C/C$ decreases monotonically by orders of magnitude as the frequency is increased into the gigahertz frequency regime and is sufficiently low to support high-precision circuit applications[20] in this frequency regime.

Figure 8 plots the La_2O_3 MIM capacitance densities *vs.* frequency. The intermediate frequency data are obtained directly from *C-V* measurements. The capacitance values at rf frequencies are extracted from the well-matched measured and modeled *S* parameters in Fig. 6a and b. La_2O_3 MIM capacitors exhibit a small drop in capacitance as the frequency is varied from 10 KHz to 20 GHz, indicating the excellence of high-*k* dielectrics formed at the low temperature of 400°C.

Figure 9 plots the dependence of the *Q* factor on frequency for high-*k* La_2O_3 MIM capacitors, whose parasitic inductance was de-

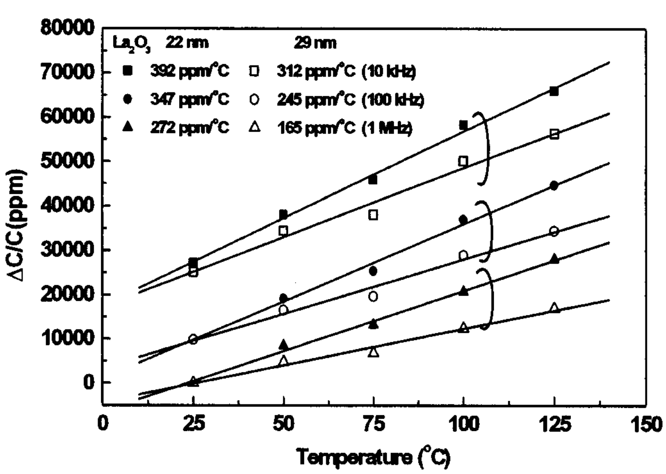

Figure 5. $\Delta C/C$ of La_2O_3 MIM capacitors as a function of temperature.

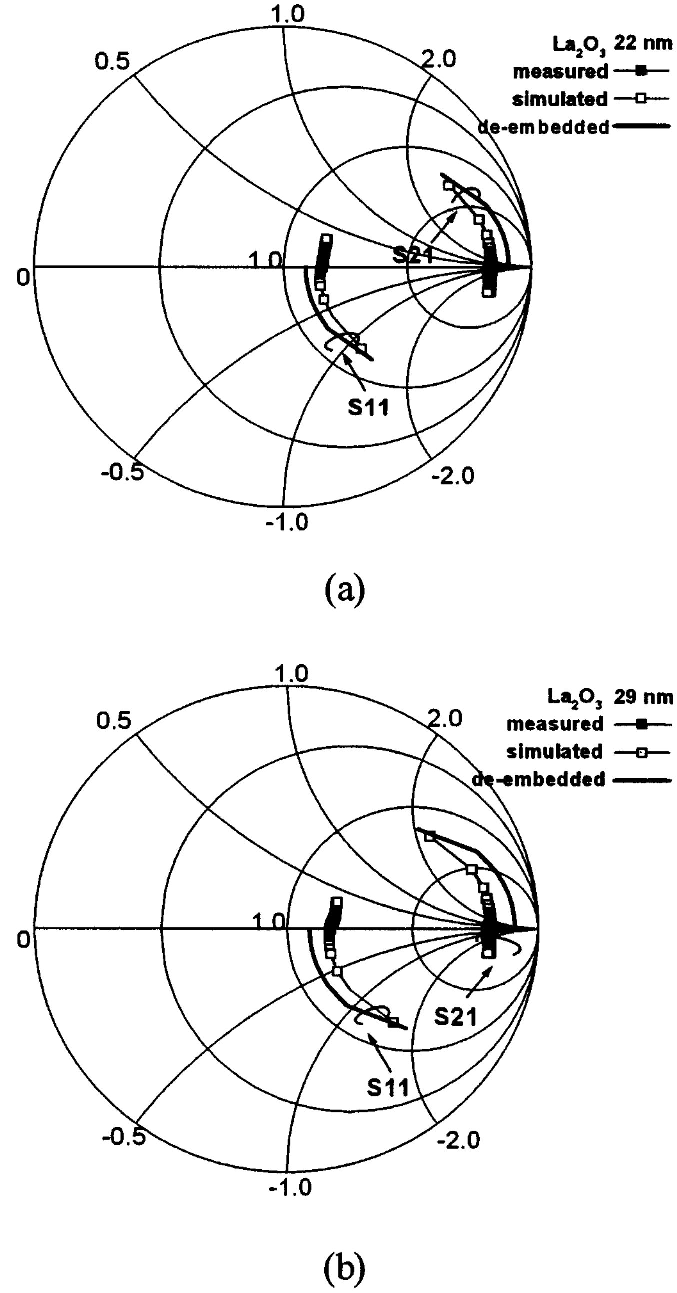

Figure 6. Measured and simulated *S* parameters of (a) 22 and (b) 29 nm La_2O_3 MIM capacitors.

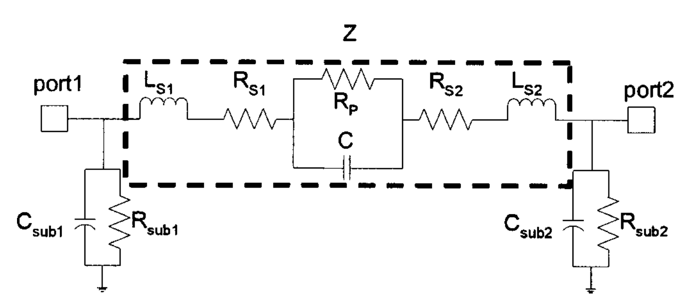

Figure 7. Equivalent circuit model used to simulate MIM capacitor in the rf regime.

Downloaded on 2014-04-27 to IP 140.113.38.11 address. Redistribution subject to ECS terms of use (see ecsdl.org/site/terms_use) unless CC License in place (see abstract).

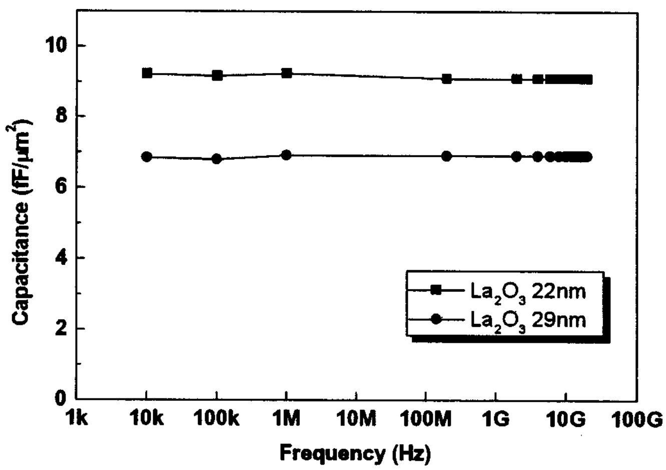

Figure 8. Frequency-dependent capacitance of La_2O_3 MIM capacitors with two dielectric thicknesses.

embedded in the through transmission line. The de-embedded Q factor is high, $\geqslant 90$, up to a resonant frequency of ~ 10 to 12 GHz. The Q factor decreases as the thickness of the dielectric falls because the resistor loss parallel to the capacitor body falls, due to the larger leakage current, as indicated by the J-V characteristics.

Conclusions

High-k La_2O_3 dielectrics were processed at 400°C to achieve a high capacitance density of 9.2 fF/μm^2 and a low $\Delta C/C \leqslant 100$ ppm at 1 GHz. A high capacitance per unity area can be maintained from 10 KHz to 20 GHz, with a large Q factor $\geqslant 90$. The good rf device integrity of high-density La_2O_3 dielectric MIM capacitors can greatly reduce the chip size of rf circuits and is useful in precision circuits at high frequencies.

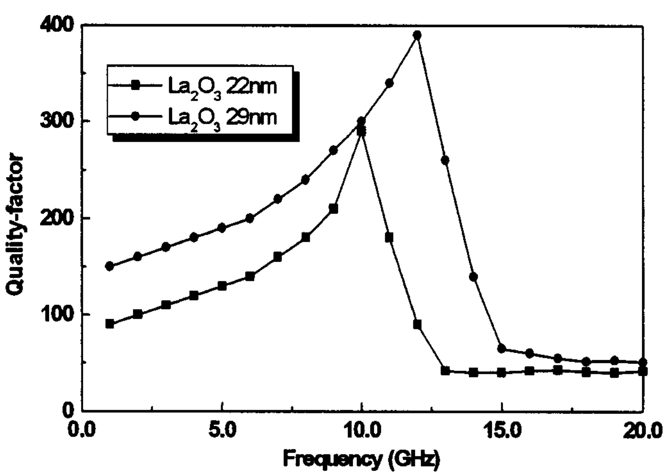

Figure 9. Quality factor of La_2O_3 MIM capacitors as a function of frequency.

Acknowledgments

The authors thank the National Science Council of the Republic of China, Taiwan, for financially supporting this research under contract no. NSC 92-2215-E-009-031. Dr. G. W. Huang at the National Nano Device Laboratory of Taiwan is appreciated for helping with the rf measurement.

National Chiao Tung University assisted in meeting the publication costs of this article.

References

1. C. H. Huang, C. H. Lai, J. C. Hsieh, J. Liu, and A. Chin, *IEEE Microwave Wireless Comp. Lett.*, **12**, 464 (2002).
2. C. H. Huang, K. T. Chan, C. Y. Chen, A. Chin, G. W. Huang, C. Tseng, V. Liang, J. K. Chen, and S. C. Chien, *IEEE RF-IC Int. Microwave Symp. Dig.*, **2003**, 373.
3. Y. H. Wu, A. Chin, C. S. Liang, and C. C. Wu, *IEEE RF-IC Int. Microwave Symp. Dig.*, **2000**, 151.
4. J. W. Lee, H. S. Song, K. M. Kim, J. M. Lee, and J. S. Roh, *J. Electrochem. Soc.*, **149**, F56 (2002).
5. S. Y. Kang, H. J. Lim, C. S. Hwang, and H. J. Kim, *J. Electrochem. Soc.*, **149**, C317 (2002).
6. C. P. Yue and S. S. Wong, *IEEE MTT-S Int. Microwave Symp. Dig.*, **1999**, 1625.
7. J. A. Babcock, S. G. Balster, A. Pinto, C. Dirnecker, P. Steinmann, R. Jumpertz, and B. El-Kareh, *IEEE Electron Device Lett.*, **22**, 230 (2001).
8. C.-M. Hung, Y. C. Ho, I. C. Wu, and K. O. , *IEEE MTT-S Int. Microwave Symp. Dig.*, **1998**, 505.
9. Z. Chen, L. Guo, M. Yu, and Y. Zhang, *IEEE Microwave Wireless Comp. Lett.*, **12**, 246 (2002).
10. J. H. Lee, D. H. Kim, Y. S. Park, M. K. Sohn, and K. S. Seo, *IEEE Microw. Guid. Wave Lett.*, **9**, 345 (1999).
11. K. Shao, S. Chu, K. W. Chew, G. P. Wu, C. H. Ng, N. Tan, B. Shen, A. Yin, and Z. Y. Zheng, in *Proceedings of 6th International Conference on Solid-State and Integrated-Circuit Technology Digest*, **2001**, 243.
12. H. Iwai, S. Ohmi, S. Akama, C. Ohshima, A. Kikuchi, I. Kashiwagi, J. Taguchi, H. Yamamoto, J. Tonotani, Y. Kim, I. Ueda, A. Kuriyama, and Y. Yoshihara, *Tech. Dig. - Int. Electron Devices Meet.*, **2002**, 625.
13. S. J. Lee, H. F. Luan, C. H. Lee, T. S. Jeon, W. P. Bai, Y. Senzaki, D. Roberts, and D. L. Kwong, in *Proceedings of Symposium on VLSI Technology*, **2001**, 133.
14. A. Chin, Y. H. Wu, S. B. Chen, C. C. Liao, and W. J. Chen, in *Digest of Symposium on VLSI Technology*, **2000**, 19.
15. M. Y. Yang, C. H. Huang, A. Chin, C. Zhu, M. F. Li, and D. L. Kwong, *IEEE Electron Device Lett.*, **24**, 306 (2003).
16. S. B. Chen, J. H. Chou, A. Chin, J. C. Hsieh, and J. Liu, *IEEE Electron Device Lett.*, **23**, 185 (2002).
17. H. Hu, C. Zhu, Y. F. Lu, M. F. Li, B. J. Cho, and W. K. Choi, *IEEE Electron Device Lett.*, **23**, 514 (2002).
18. S. B. Chen, J. H. Chou, A. Chin, J. C. Hsieh, and J. Liu, *IEEE MTT-S Int. Microwave Symp. Dig.*, **2002**, 201.
19. C. H. Huang, M. Y. Yang, A. Chin, C. X. Zhu, M. F. Li, and D. L. Kwong, *IEEE MTT-S Int. Microwave Symp. Dig.*, **2003**, 507.
20. C. Zhu, H. Hu, X. Yu, A. Chin, M. F. Li, and D. L. Kwong, *Tech. Dig. - Int. Electron Devices Meet.*, **2003**, 879.
21. K. T. Chan, A. Chin, C. M. Kwei, D. T. Shien, and W. J. Lin, *IEEE MTT-S Int. Microwave Symp. Dig.*, **2001**, 763.
22. K. T. Chan, A. Chin, Y. B. Chen, Y.-D. Lin, D. T. S. Duh, and W. J. Lin, *Tech. Dig. - Int. Electron Devices Meet.*, **2001**, 903.
23. Y. H. Wu, A. Chin, K. H. Shih, C. C. Wu, C. P. Liao, S. C. Pai, and C. C. Chi, *IEEE MTT-S Int. Microwave Symp. Dig.*, **2000**, 221.
24. T. Park, H. J. Cho, J. D. Choe, S. Y. Han, S.-M. Jung, J. H. Jeong, B. Y. Nam, O. I. Kwon, J. N. Han, H. S. Kang, M. C. Chae, G. S. Yeo, S. W. Lee, D. Y. Lee, D. Park, K. Kim, E. Yoon, and J. H. Lee, *Tech. Dig. - Int. Electron Devices Meet.*, **2003**, 27.

Downloaded on 2014-04-27 to IP 140.113.38.11 address. Redistribution subject to ECS terms of use (see ecsdl.org/site/terms_use) unless CC License in place (see abstract).